MDPI

Communication

Improved Target Laser Capture Technology for Hexagonal Honeycomb Scanning

Bing Jia, Fan Jin * , Qiongying Lv and Yubing Li

College of Mechanical and Electrical Engineering, Changchun University of Science and Technology, Changchun 130012, China
* Correspondence: jf1064yx@163.com

Abstract: In laser tracking systems, capturing moving targets is a prerequisite to guaranteeing a tracking system's performance. Previous studies have confirmed that the capture probability of hexagonal spiral scanning is higher than that for other scanning methods, but there is still room for improvement. This article proposes an improved hexagonal honeycomb scanning capture method based on hexagonal spiral scanning for a prior moving target model with a Gaussian distribution positioned within the scanning range of the visual threshold. Through experimental verification, it was found that, within the same scanning field of view, the capture probability can be increased by 3% compared to that in traditional hexagonal spiral scanning, making the capture probability greater than 98%. The improved hexagonal honeycomb structure scanning method proposed in this article provides a new solution for target acquisition problems in fields such as laser communication, laser docking, and airborne radar.

Keywords: moving target model capture; laser scanning; improved hexagonal honeycomb structure scanning

1. Introduction

Laser scanning is a topic that is extremely broad in scope. A scanning system can track objects by capturing reflected light or by fluorescing the image and acquiring the fluoresced light. The output system directs light to produce images for marking [1]. Laser scanning capture technology has been widely studied and applied in many engineering fields due to its ability to accurately and directly scan small targets.

In the field of biology, the main applications of laser scanning capture include subcellular protein localization [2], the imaging of biological surfaces [3], trapping light-absorbing microparticles in the air [4,5], bright-field light microscopy [6] and trapping nanoparticles on the surfaces of solutions [7]. In the medical field, research and development on technologies such as laser capture microdissection [8,9], the laser capture of individual cells in complex tissues [10], laser capture cell sampling [11], the analysis of gene expression profiles using laser capture microdissection [12], and the laser capture of blood cells [13] has demonstrated that laser capture technology has profound significance for medical progress and for the treatment of major diseases. In the engineering field, laser scanning acquisition is mainly used in laser radar, mechanical engineering, the space industry, and other fields, such as 3D nanofabrication [14], high angular resolution LiDAR [15], super-resolution laser probing [16], laser printing [17], and laser scanning [18,19]. However, in actual engineering applications, the problems of environmental complexity and spatial instability exist, posing new challenges for laser capture and tracking systems.

This article focuses on the field of laser communication and conducts research on the capture of moving targets. The measurement of dim or small moving targets in complex environments calls for high sensitivity, high precision and high angular deflection velocity in the visual axis for traditional single-station measuring equipment. The laser tracking

measurement system has been proposed as a new type of measurement system with high measurement accuracy, a wide measurement range, and high pointing accuracy, and has thus become a global research hotspot in target tracking technology.

The premise of maneuvering tracking is to establish an accurate target model and then, based on a variety of filtering tracking algorithms, effectively estimate the target's position in the next step. Whether visual sensors or laser detection methods are used, target capture is the first step in the target tracking process.

Common scanning methods in laser tracking systems include rectangular branch scanning, rectangular spiral scanning, circular spiral scanning, hexagonal spiral scanning, etc. These scanning methods are used in laser communication, satellite docking, airborne radar, and other fields. The scanning mode and scanning parameters used in a photoelectric detection system are of great significance when it comes to improving the detection accuracy, detection efficiency, and target acquisition probability of the laser tracking system. In previous studies, photoelectric scanning detection models played an important role in monitoring low, slow, and small targets in the air, enabling the efficient capture of moving targets [20]. A rectangular spiral scanning method based on spiral scanning [21] has been proposed for space rendezvous lidar target acquisition technology that simplifies the system's structure, reduces system difficulty, and increases acquisition probability [22]. In previous studies on the use of radar scanning in space laser communication, it was concluded that uniform sinusoidal spiral scanning has greater advantages [23], but this scanning method has a complex control process for galvanometer laser scanning [24–26]. In addition, some studies have compared several common scanning methods and found through theoretical analysis and simulation experiments that hexagonal spiral scanning has advantages that are different from those of other scanning methods [27,28]. When the moving target's position is combined with a Gaussian distribution model, the capture probability using rectangular spiral scanning is 85.80%, and the required number of light feet is 81; the capture probability using rectangular branch scanning is 62.48%, and the required number of light feet is 81; and the acquisition probability using hexagonal spiral scanning is 87.79%, and the number of light feet required is 61. The acquisition speed of hexagonal spiral scanning is, therefore, the fastest.

The sampling frequency in laser tracking systems is also an important factor. When the sampling frequency of the target increases, the acquisition probability of hexagonal spiral scanning and rectangular spiral scanning increases steadily, and the acquisition probability of hexagonal spiral scanning is the highest out of all methods. Moreover, changes in the sampling frequency have a great impact on the rectangular branch scanning. Due to improvements in the sampling frequency, the branch scanning method starting from the edge can capture a moving target at the center of the field of view more quickly. If the laser sampling frequency is not high enough when the laser reaches the center of the field of view, the target will have moved outside of the field of view, that is, the acquisition probability will be extremely low. There is a peak before and after the sampling frequency reaches 30 kHz wherein the acquisition probabilities of hexagonal spiral scanning and rectangular spiral scanning show a certain decline. This indicates that when the sampling frequency increases, the spiral scanning spot moves faster to the edge of the field of view, resulting in a small reduction in the acquisition probability. The acquisition probability of rectangular branch scanning tends to be stable, indicating that it is not restricted by the sampling frequency but by the scanning method itself.

For a moving target with a high probability of appearing in the center of the field of view, the hexagonal spiral scanning mode and the target cannot be effectively matched in the time domain and space domain. Based on the above research, combined with the research background, this paper proposes an improved hexagonal scanning mode—called improved hexagonal honeycomb structure scanning—which establishes a prior motion model with a Gaussian distribution in the threshold scanning range. In the same scanning field of view, the acquisition probability is higher than that of traditional hexagonal spiral scanning.

2. Improved Scan Capture Model with a Hexagonal Honeycomb Structure

2.1. Establishment of the Improved Hexagonal Honeycomb Structure Scanning Model

At present, most hexagonal scanning methods available in the literature are hexagonal spiral scanning methods; the principle of this method is similar to spiral scanning and zigzag scanning [29–31]. They all scan from the center to the 2π direction. Based on the research of [20], it was concluded that when the position where the target enters the visual threshold range for the first time is modeled with a Gaussian distribution and different scanning methods are used to cover and determine the visual field, the hexagonal spiral scanning method has a higher acquisition probability than the circular and rectangular methods.

To further improve the target acquisition probability of laser tracking systems and make the detection spot appear in the center more often, this paper proposes a new hexagonal scanning method—the improved hexagon honeycomb structure scanning model. Different from traditional spiral scanning with an increasing hexagonal radius, the scanning of the hexagonal honeycomb structure is improved by first completing the hexagon of the smallest unit and then scanning from the inside to the outside. This method achieves detection in the center of the field of view more often and reduces the number of times target capture occurs outside the field of view. For moving targets with a Gaussian distribution, the scanning mode of the improved hexagonal honeycomb structure is the same as the spiral scanning mode, which starts scanning from the area with the highest probability of target occurrence. At the same time, this mode makes up for the defect of missing scanning of the outer circle of spiral scanning and can repeat the spiral scanning of the inner circle.

Assume that the pulse frequency matches the scanning frequency, that is, the laser sends out a pulse every time the galvanometer jumps. Then, define a visual scanning range threshold. The scanning mode is shown in Figure 1. In the figure, a circle is used to represent the light foot generated by a pulse, and an overlapping hexagon is used to represent the path of the laser spot's center. The darker the color, the more overlaps there are.
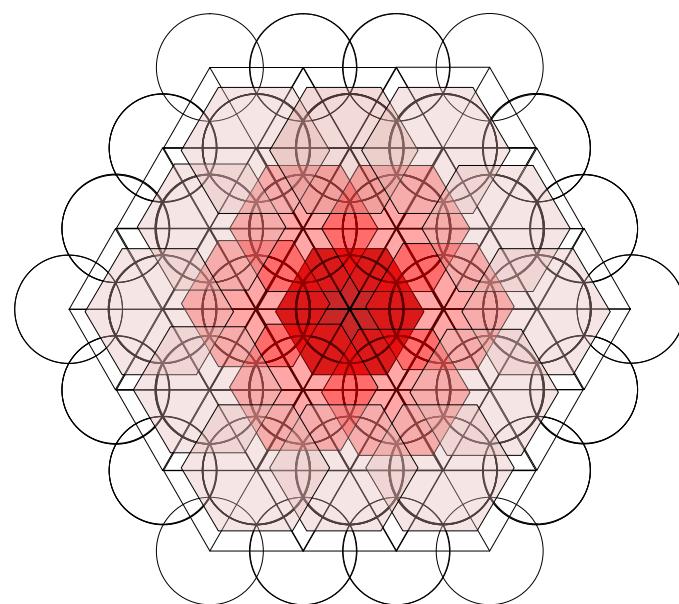

Figure 1. Schematic diagram of improved hexagonal honeycomb scanning structure.

The scanning path of the improved hexagonal honeycomb structure is briefly described below:

(1) First, form a light foot at the origin at the center of the scanning field, then scan along the regular hexagon edge of the center to form the first layer of light feet with six vertices as the centroid;

(2) Take the vertex of the central regular hexagon as the centroid and make six regular hexagons. The scanning track is the edge of the six regular hexagons, scanning out the second layer of light feet;

(3) The apex of the hexagon is formed after the second layer of scanning, and the bisection points of each side are taken as the hexagon centroid. Its edges are scanned in turn to generate the third layer of light feet, and so on.

According to the scanning mode shown in the figure, it can be seen that the optical foot density and coincidence rate in the center of the field of view are higher. Under a normal distribution of the target and determination of the field of view's size, compared with other scanning methods, the target is more likely to be captured using this scanning mode.

Therefore, the scanning path of the improved hexagonal honeycomb scanning structure is modeled. First, define the center position of the current flare. The vector groups A, B, C, D, E, and F of starting point O have included angles of 60° between their adjacent vectors, and the vectors' lengths are equal to the side length of the regular hexagon of the path. The model is shown in Figure 2.
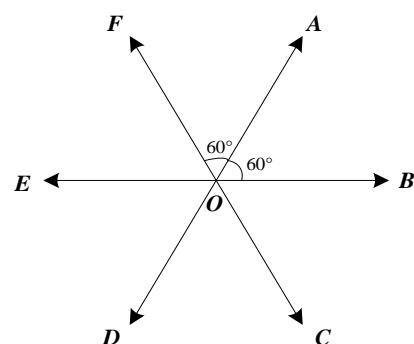

Figure 2. Six-direction scanning path vector.

The scanning path of the light spot is represented by a vector. If the included angle between the light foot and the horizontal right is 60° from the central position O of the light spot, and the length is r, it is represented by vector A. It can be seen that the scanning path vector satisfies the relationship of $A = -D$, $B = -E$, and $C = -F$. That is, if the trajectory follows the vector of $A + B + C + D + E + F$, and the light foot position returns to the starting point.

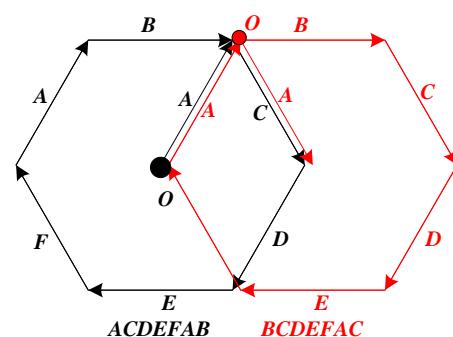The scanning path vector of the first optical foot is shown in Figure 3.

Figure 3. Vector representation example of the first layer optical foot scanning path.

Starting from the origin O of the scanning field of view, the optical foot conducts a scan around O to obtain the first optical foot. Its path description vector is $A + C + D + E + F + A + B$, abbreviated as ACDEFAB. From the above-mentioned path $A = -D, B = -E, C = -F$, the path description can be simplified to obtain the end position A of the optical foot relative to the origin after the path scanning as follows:

$$A + C + D + E + F + A + B = -D - F + D + E + F + A - E = A \tag{1}$$

This process is shown in the black path in Figure 3. Here, the accumulation of seven vectors is uniformly used to represent one regular hexagonal path scan, and the second regular hexagonal path scan is performed using the end position A of the first scan as the starting point. Then, the second path's description vector is $B + C + D + E + F + A + C$, abbreviated as *BCDEFAC*, as shown in the red path in Figure 3. Table 1 shows the scanning path of the first optical foot.

Table 1. Scanning path of first layer of optical feet.

Number	Staring Point	Path Vector
0	*O*	*ACDEFAB*
1	*A*	*BCDEFAC*
2	*B*	*CDEFABD*
3	*C*	*DEFABCE*
4	*D*	*EFABCDF*
5	*E*	*FABCDEA*
6	*F*	*ACDEFAB*

In the table, the optical foot scanning path No. 0 represents the hexagonal path with the scanning field origin as the centroid. The optical foot scanning path from No. 1 to No. 6 is the scanning path of the first layer of optical feet. The starting point is marked with vector coordinates relative to the origin. The starting point position of the current serial number is the last ending point position, which can be obtained by adding the last starting point vector and the path description vector. For example, the starting point of track No. 2 is the coordinate of the *B* vector, the path description vector is *CDEFABD*, and the starting point method for finding the No. 3 track is (Figure 4):

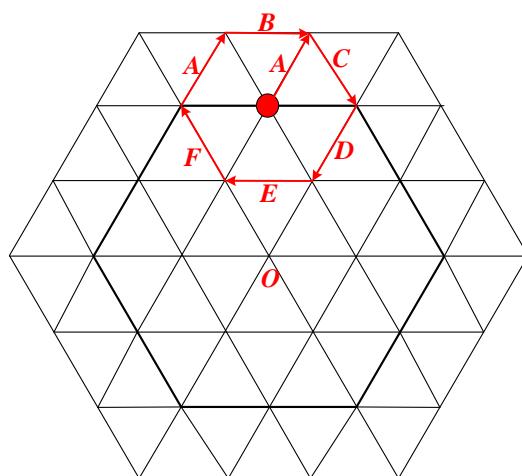$$B + (C + D + E + F + A + B + D) = C \tag{2}$$

Figure 4. Schematic diagram of a regular hexagon in the first scan.

Table 2 shows the scanning track of the second optical foot.

Table 2. Scanning path of the second layer of optical feet.

Number	Starting Point	Path Vector
1	*AF*	*ACDEFAB*
2	*AA*	*BCDEFAC*
3	*AB*	*BCDEFAC*
4	*BB*	*BCDEFAC*
5	*BC*	*CDEFABD*
6	*CC*	*CDEFABD*
7	*CD*	*DEFABCE*
8	*DD*	*DEFABCE*
9	*DE*	*EFABCDF*
10	*EE*	*EFABCDF*
11	*EF*	*FABCDEA*
12	*FF*	*FABCDEA*

Due to the different methods of selecting the starting point of the second layer scanning path, the path vectors with serial numbers 1 and 2 have special properties. The other path description vectors are the same as the path description vectors with serial numbers 2 to 6 in the first layer, and they cycle once at the hexagon bisection point. This path description vector is extended to the scanning path of the third layer, and the corresponding path description vector of the first layer is cycled three times at the outermost regular hexagonal trisection point to obtain the three-layer light foot scanning path.

2.2. Capture Conditions

The controllable factors affecting the comprehensive probability of the laser tracking system capturing the target include the galvanometer scanning mode, the laser sampling frequency, and the laser divergence angle. The capture probability refers to the likelihood that the laser is scattered by the target and received by the receiving optical system within the laser's single frame scanning area. As long as the signal is received, it is determined that the target is captured. After the target enters the field of view, appropriate scanning system parameters are selected to complete the target acquisition, so that the maximum probability of the target falling into the visual range of the receiving system is achieved. Acquisition systems using other working modes, such as microwave radar, can scan the detection airspace in all directions, without considering the scanning speed. The laser acquisition and tracking system of the TOF measurement system selected in this paper is based on the matching of the time sequence and space to complete target acquisition. Therefore, the need to model the two kinds of independent random processes of the target and scanning systems based on a time sequence must be considered in the simulation and verification process.

The capture diagram of a moving target and the proposed detection model are shown in Figure 5, in which the measured target enters the detection area from the left side.

To simplify the complexity of the model, when a galvanometer-type photoelectric detection model is scanned for one frame, the time when the target enters the field of view is exactly the time when the detection model starts scanning; that is, the time when the random target enters the field of view and the time when the detection model scans for one frame are both T, which are set in the same detection area. When modeling a moving target, the following points should be obeyed:
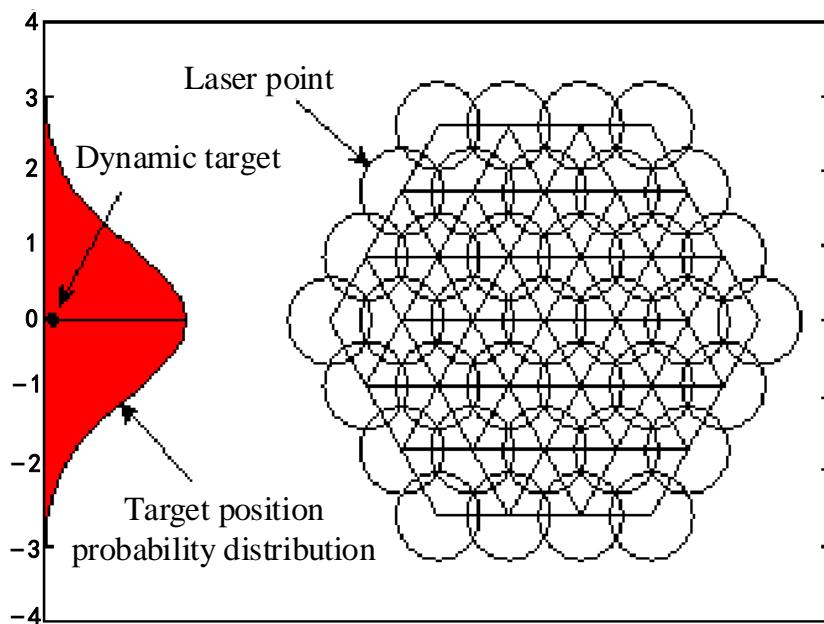
Figure 5. Schematic diagram of maneuvering target and detection model acquisition.

(1)   The target motion model is an inertial target model;
(2)   The scanning field of view position is the best estimation prior result;
(3)   The target time location in the two-dimensional plane is Gaussian white noise, that is, it obeys a Gaussian distribution;
(4)   The noise in the z direction is not considered.

2.3. Scanning Step Size Analysis

During galvanometer scanning, the scanning point's step size has a great impact on moving target acquisition. If the step size is too large, some scanning areas will be missed, reducing the acquisition probability, as shown in Figure 6a. Too small a step size will increase the scanning repetition rate and capture time, as shown in Figure 6b. To achieve fast and efficient scanning, the optimal scanning step size that completely covers the capture uncertainty area must be selected. The scanning beam can not only eliminate missed scanning areas but also reduce invalid overlapping scanning areas, as shown in the center circle of Figure 6c.
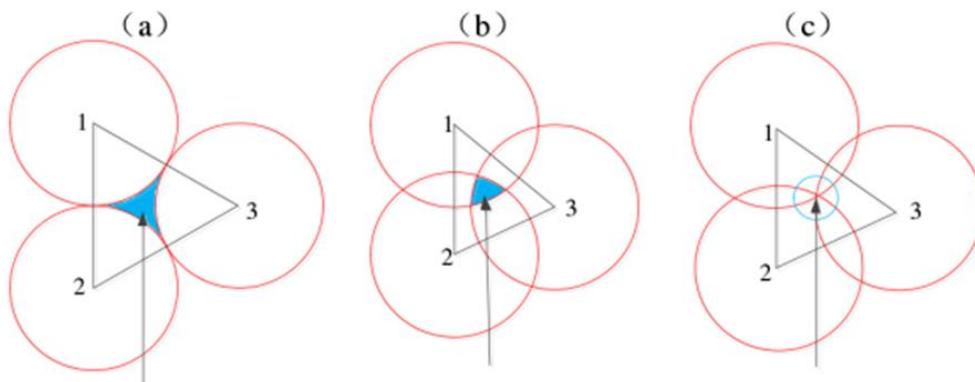

Figure 6. Schematic diagram of scanning results when different scanning steps are selected: (**a**) spot tangency, (**b**) spot intersection, (**c**) center intersection.

The numbers in Figure 6. represent the scanned light feet. When the points are tangent, a missed scan area in the blue area will appear in the middle, reducing the capture probability; When the points intersect, a repeating area with a blue part will appear in the

middle, increasing the scanning time; When the centers intersect, the scanning efficiency is highest.

The projection of the laser light foot on the scanning area is shown in Figure 7. Assume that the laser beam's divergence angle is γ, the laser spot's diameter is d', and the step size of two adjacent spots is φ. At this time, the light spot offset distance is d'_x and d'_y. When φ is less than the maximum step size φ_{max}, the laser spots overlap. Since γ is of the order of mrad, the projection areas of two adjacent laser spots are regarded as circles with the same diameter. In rectangular spiral scanning, if the coverage area of the spot is rectangular, as shown in Figure 7a, the scanning field of view is S at this time:

$$S = d'_x \times d'_y \tag{3}$$
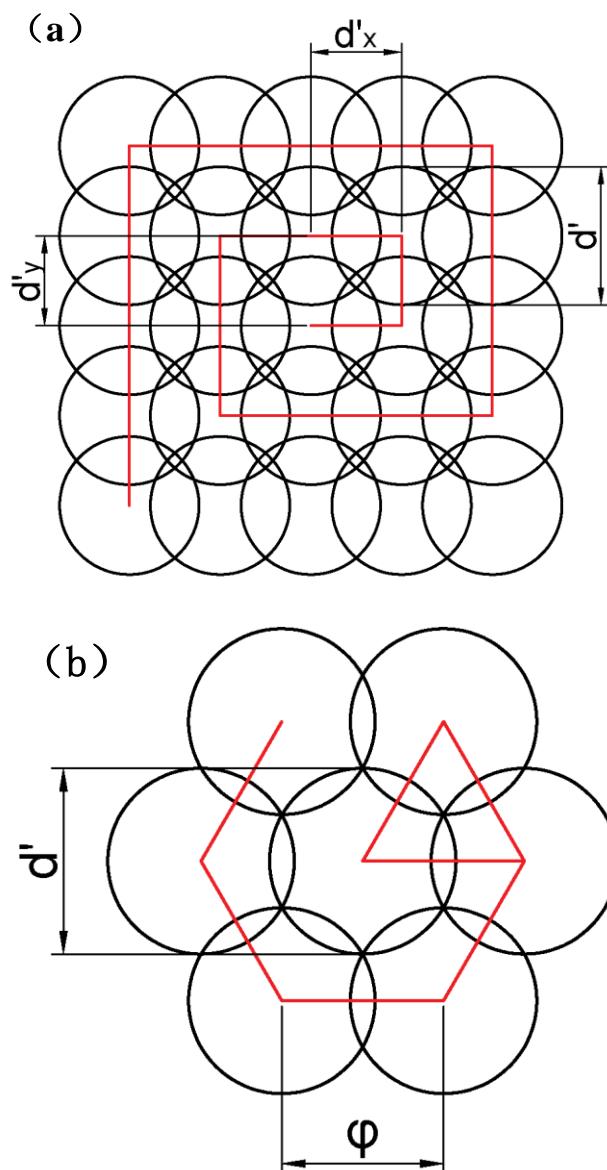
$$d'^2_x + d'^2_y = d'^2 \tag{4}$$

Figure 7. Schematic diagram of scanning compensation: (**a**) rectangular scanning area; (**b**) hexagonal scanning critical area.

Therefore, when and only when $d'_x = d'_y = \sqrt{2}/2d'$ has the largest area of S, according to the scanning relationship, the step size of the scanning point is $\varphi = \sqrt{2}/2d'$.

In hexagonal spiral scanning and hexagonal edge equidistant spiral scanning, the overlapping area of the light beam is small, as shown in Figure 7b. At this time, the step size of the scanning point is $\varphi = \sqrt{3}/2d'$ according to the scanning relationship.

3. Comparison and Analysis of Scanning Capture Models

To verify the above analysis, this paper adopts a TOF laser detection system and two-dimensional high-speed galvanometer scanning to obtain spatial information. On the one hand, the target acquisition probability should be considered in the scanning process, and on the other hand, the difficulty of the control method of a two-dimensional mechanical galvanometer should be considered. Therefore, the rectangular scanning and hexagonal scanning models should be analyzed and compared first, as follows (Figures 8–11):

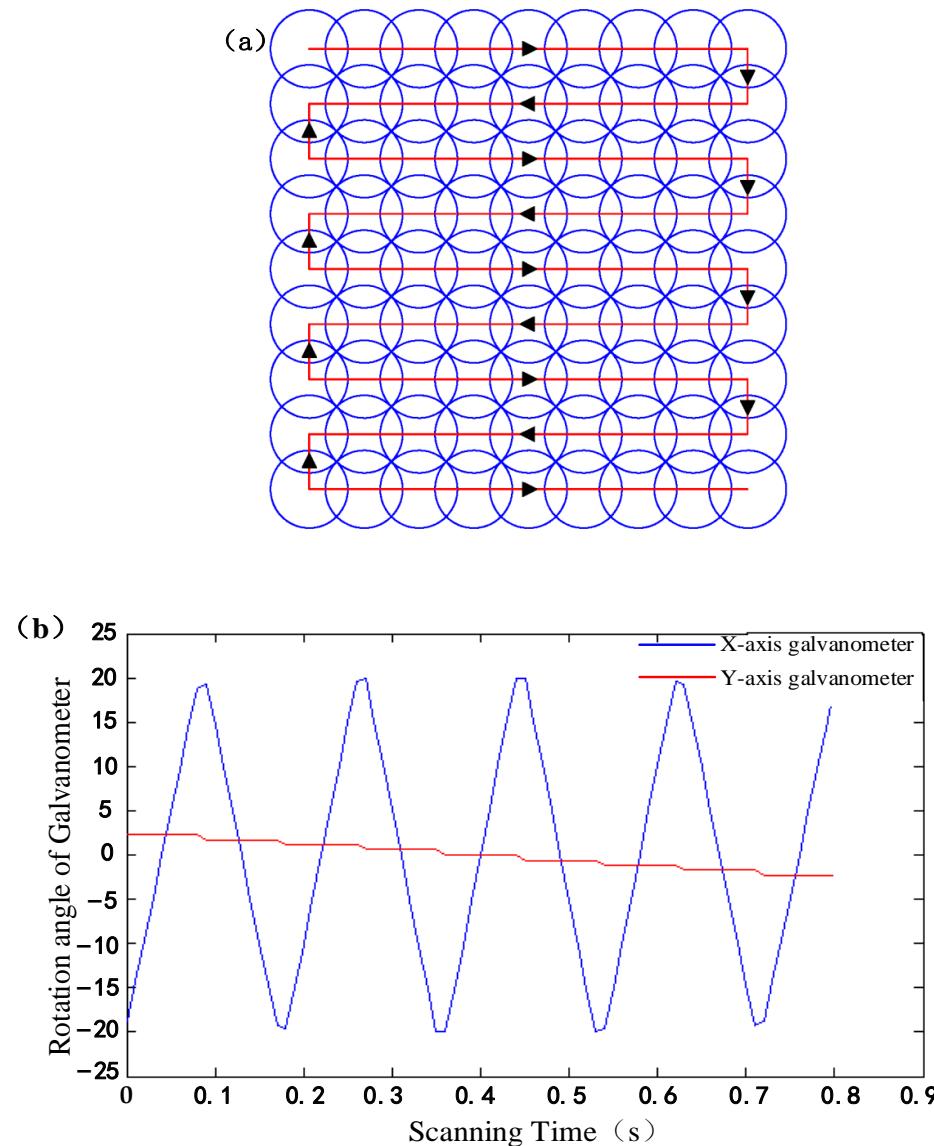(1) Simulation analysis of rectangular scanning

Figure 8. Rectangular scanning: (**a**) schematic diagram of rectangular scanning path; (**b**) schematic diagram of the galvanometer's deflection angle.
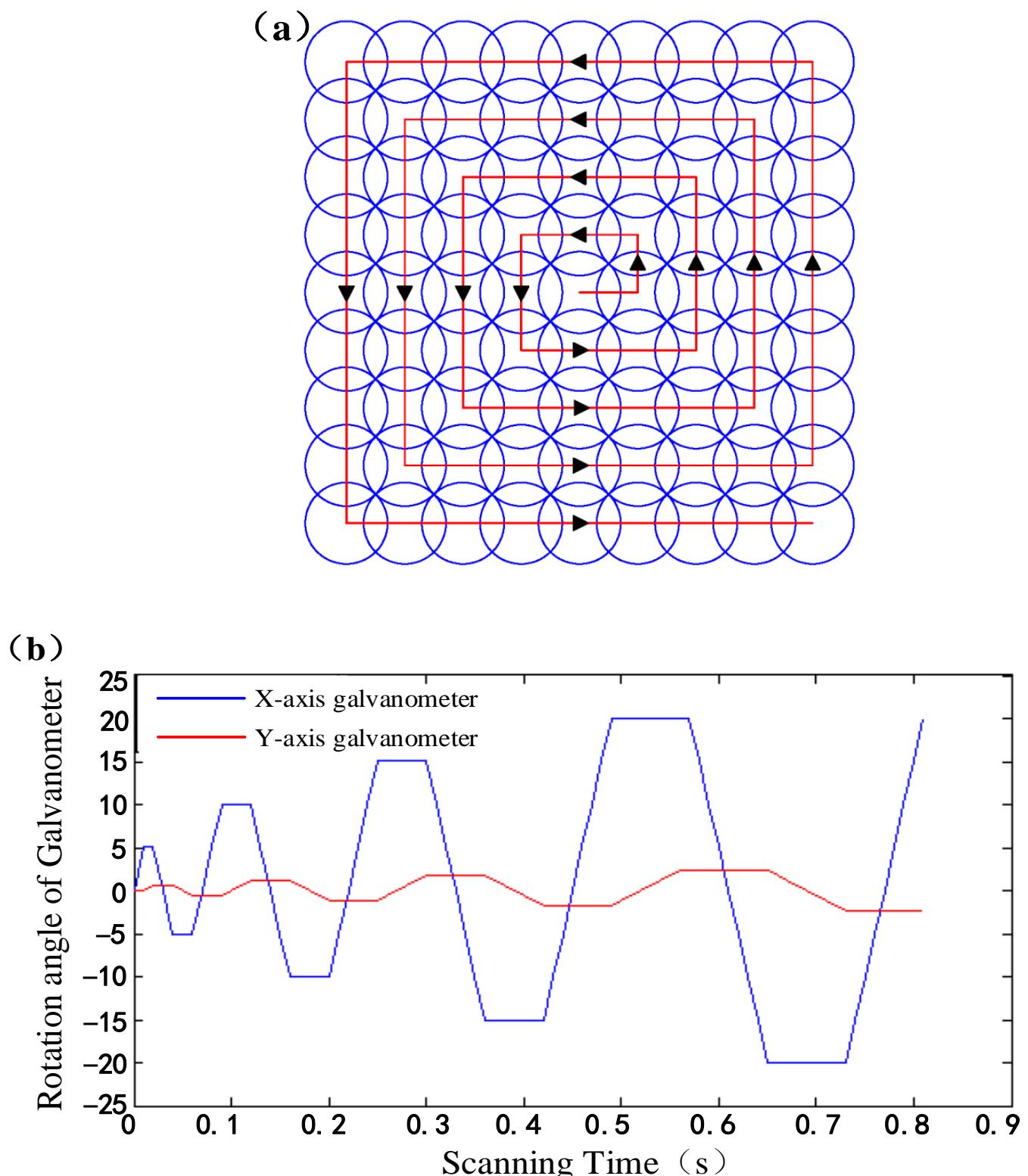
（a）

（b）

Figure 9. Rectangular spiral scanning: (**a**) schematic diagram of rectangular spiral scanning path; (**b**) schematic diagram of the galvanometer's deflection angle.
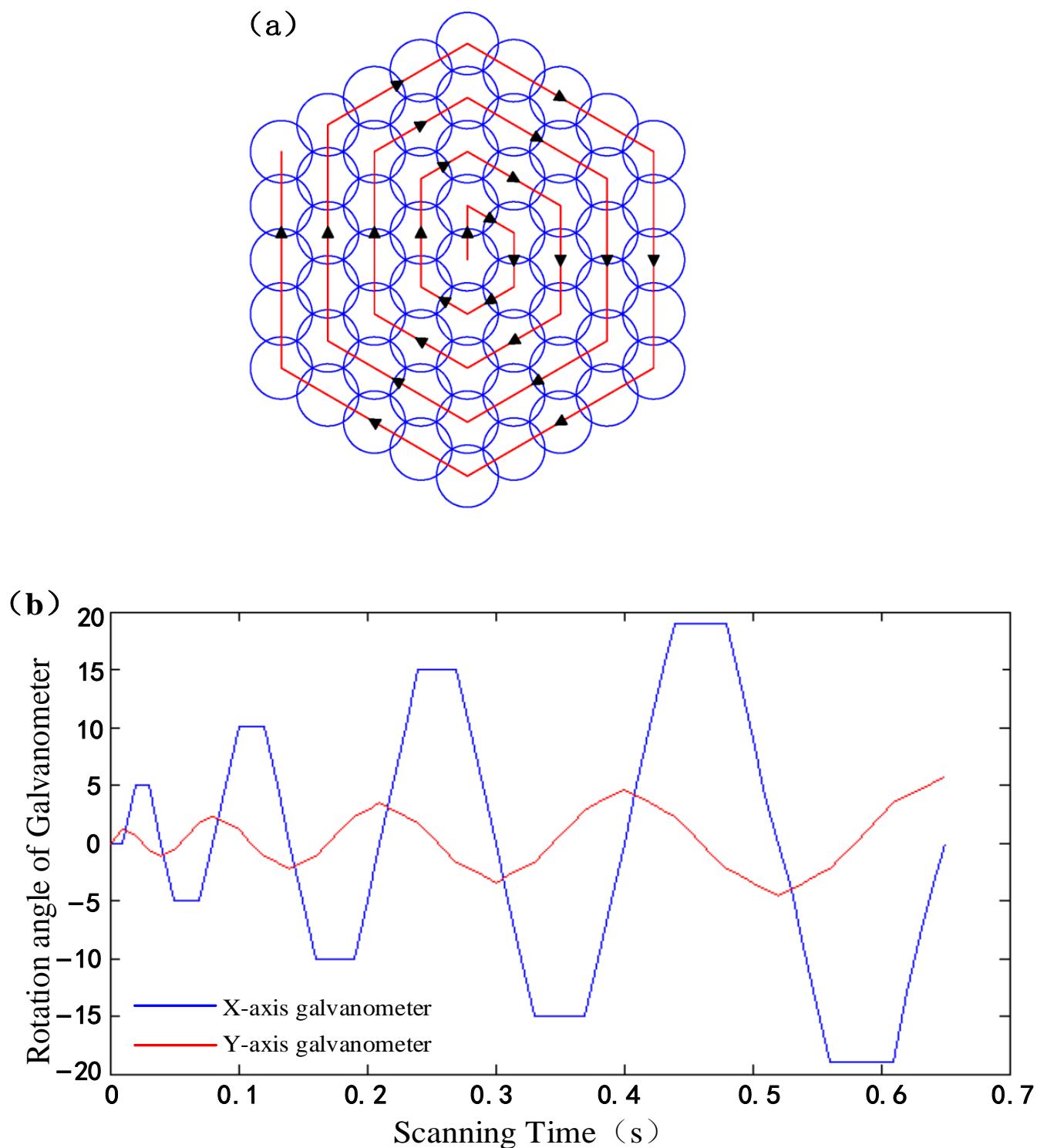
(2) Simulation Analysis of Hexagonal Scanning

（a）

（b）

Figure 10. Hexagonal spiral scanning: (**a**) schematic diagram of hexagonal scanning path; (**b**) schematic diagram of the galvanometer's deflection angle.
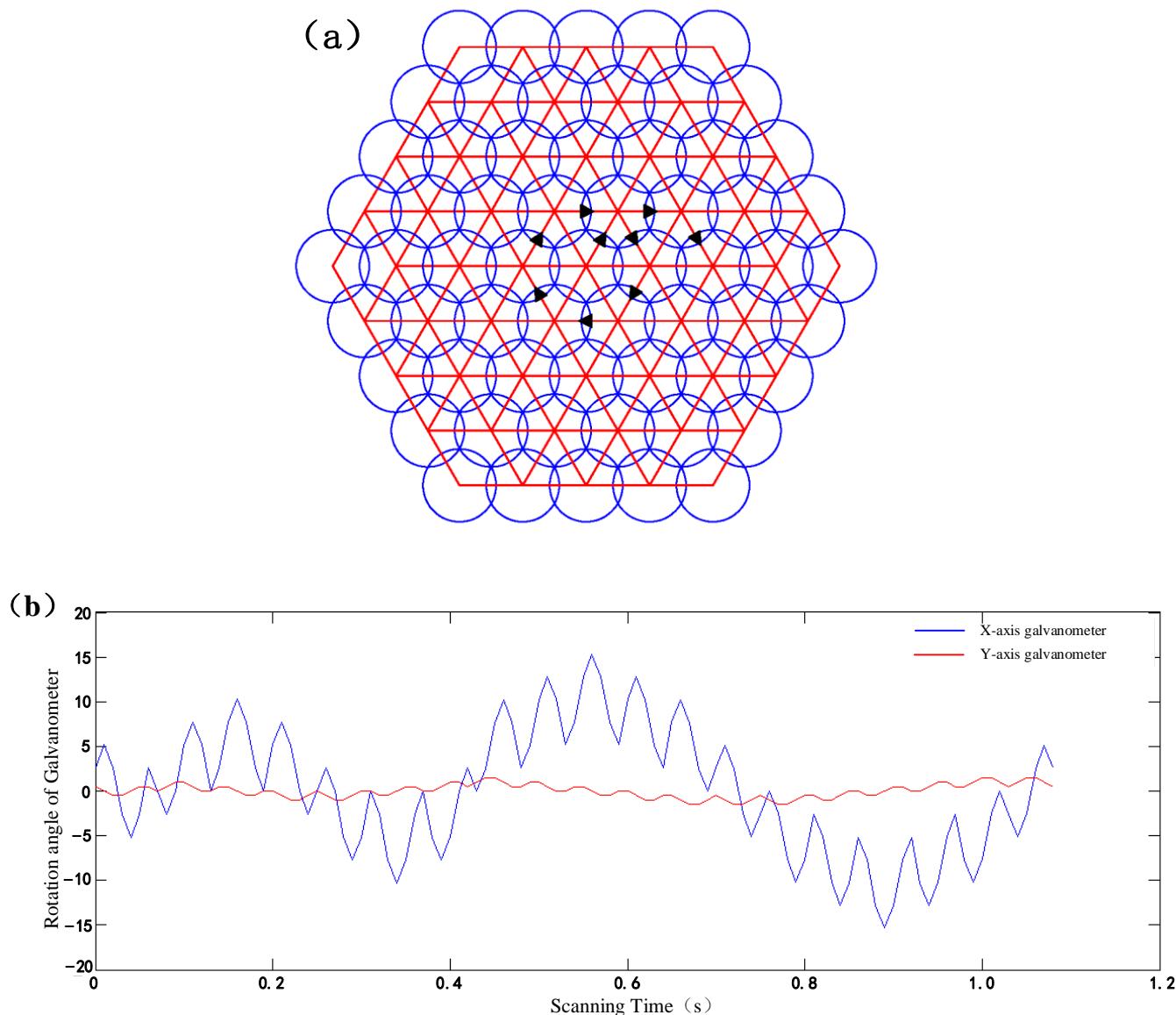
Figure 11. Improved hexagonal honeycomb structure scanning: (**a**) schematic diagram of scanning path of improved hexagonal honeycomb structure; (**b**) schematic diagram of the galvanometer's deflection angle.

The improved hexagonal honeycomb structure scans the inner circle more times within a visual threshold, so the scanning time is greater than traditional hexagonal spiral scanning. The simulation results show that the scanning amplitude of the honeycomb structure is smaller than that of traditional hexagonal spiral scanning, and the capture rate is also higher than that of the traditional method. The step size of the honeycomb structure does not change, which makes it easier to control the high-speed galvanometer system.

4. Experimental Simulation

To verify that the improved hexagonal honeycomb structure scanning method can improve the capture times of moving targets, this paper uses the control variable method to carry out a simulation and comparative analysis of four scanning methods.

Let the moving target speed of the CV model be 100 m/s, the laser output frequency be 10 kHz, the laser beam divergence angle be 10 mrad, the spot diameter be 25 mm, the step lengths of rectangular scanning and rectangular spiral scanning be 1.66 mm, and the step lengths of hexagonal spiral scanning and hexagonal honeycomb structure scanning be

3.15 mm. The distance R between the defined target point and the laser detection center point satisfies the formula:

$$|R| = \sqrt{(\Delta x)^2 + (\Delta y)^2} = \sqrt{|x(t_i) - x(t)|^2 + |y(t_i) - y(t)|^2} \qquad (5)$$

where $y(t_i) = normrad(0, 1, 1, 1)$ is a random number.

When the target is captured successfully, the spatial relationship between the photodetector and the target is shown in Figure 12, and the distance R between a single optical foot and the target point within the scanning threshold meets the following requirement:

$$|R| < |\lambda\delta| \qquad (6)$$

where λ is the receiving field angle of the target detector, and δ is the plane distance between the target and the scanning visual threshold.
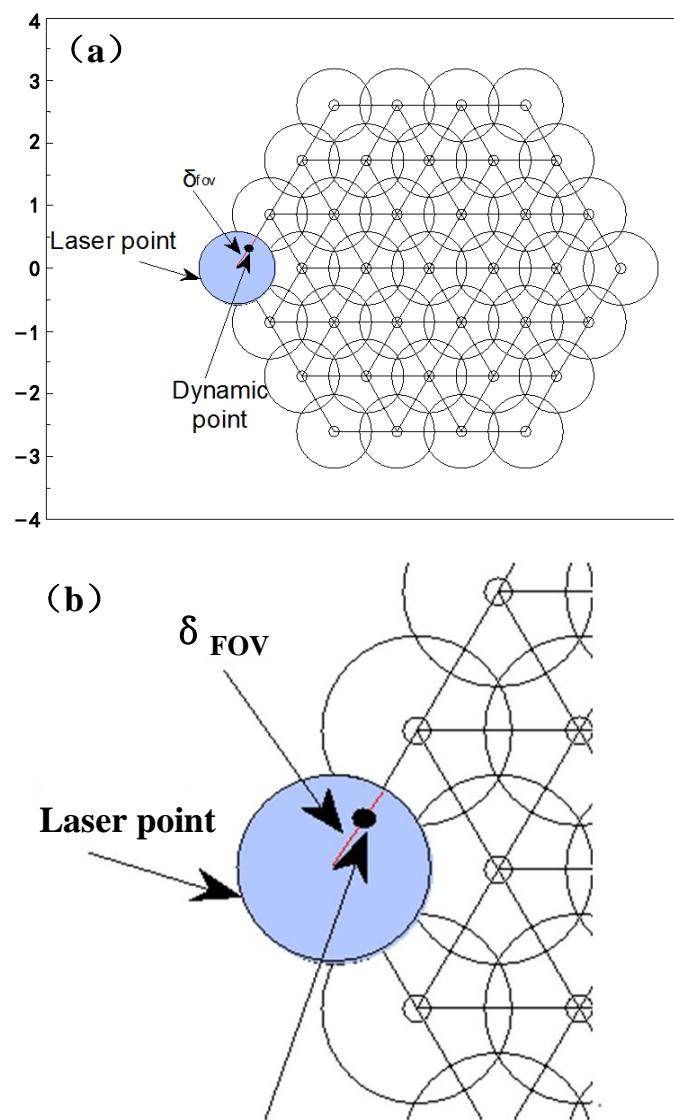

Figure 12. Schematic diagram of successful target acquisition. (**a**) Schematic diagram of spatial relationship between detector and target. (**b**) The relationship between a single light foot and the target point.

Matlab Simulink simulation software was used to establish simulation models for the four scanning methods; Monte Carlo simulations were used for capture analysis;

1000 single field scans were conducted for each scanning method; and the proportion of single field scanning capture times of each scanning method to the total scanning times was output.

The acquisition results obtained after the simulation are shown in Figure 13. From the simulation results in Figure 13, it can be concluded that when the target has been scanned 1000 times in a single field, the proportion of moving targets being captured by traditional hexagonal spiral scanning one to two times is large, 0.547 and 0.425, respectively. One moving target being captured by rectangular spiral scanning accounts for a large proportion, of 0.623. The proportions of two to three mobile targets being captured by rectangular branch scanning are 0.235 and 0.426. The proportion of two to four mobile targets captured by the improved hexagonal honeycomb structure scanning is larger, being 0.308, 0.285, and 0.298. The proportion of targets not captured after scanning a frame is smaller than that of other models. It can be seen from Figure 14 that when a target enters a fixed field of view, it is captured when it is detected more than or equal to one time. The maximum acquisition probability of the improved hexagonal honeycomb structure is 99%, followed by the hexagonal spiral scan at 96% and the rectangular spiral scan at 94%. The minimum acquisition probability is obtained by the rectangular branch scanning method, at 85%.
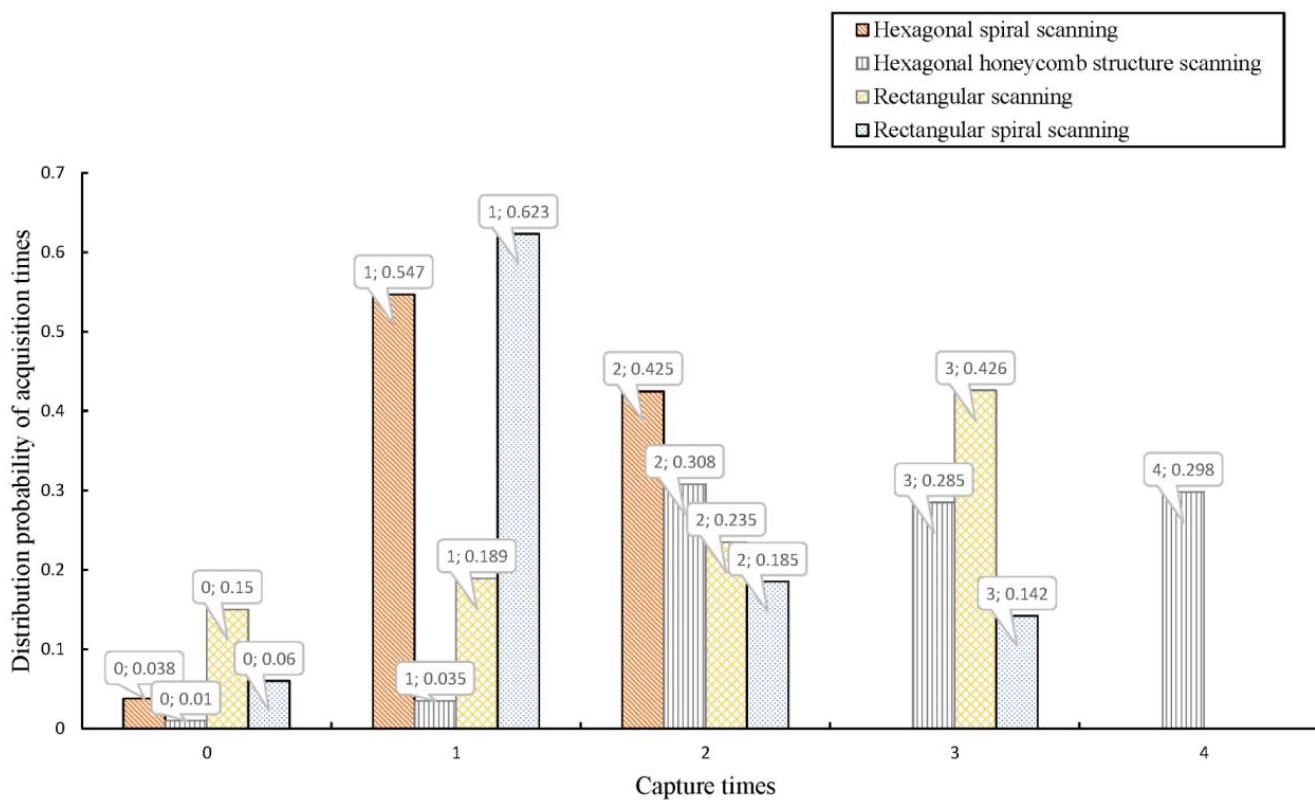

Figure 13. Capture probability simulation results of 1000 scans per field.
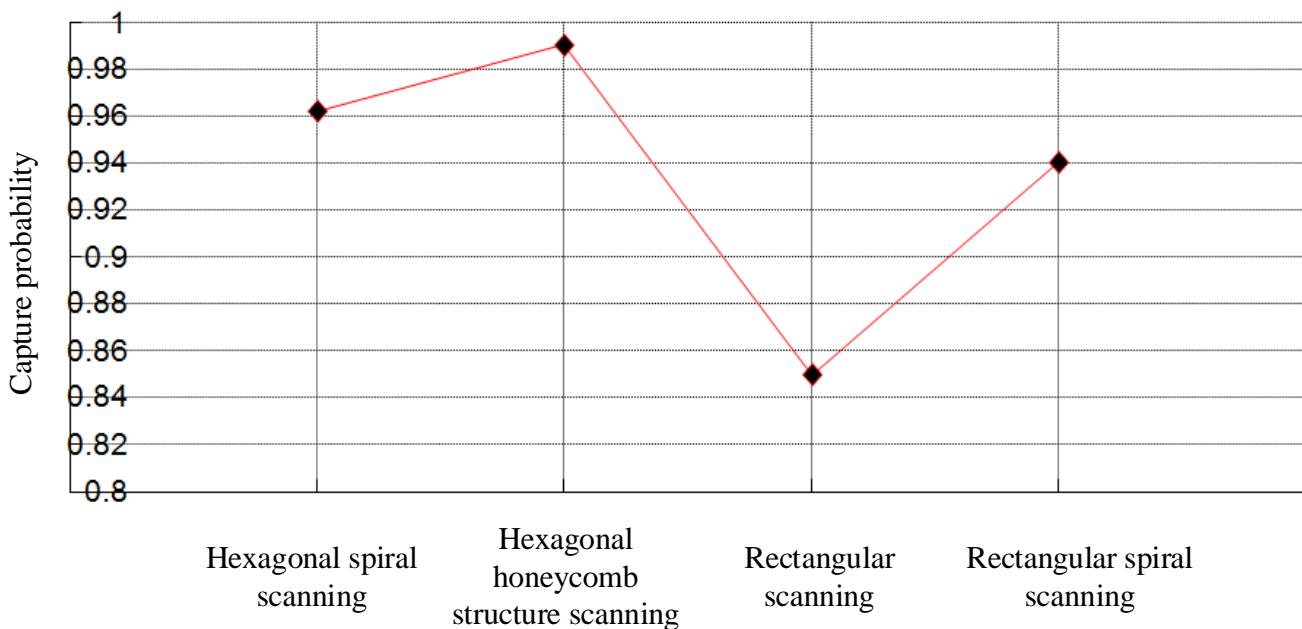
Figure 14. Analysis of capture probability simulation results.

When 1000 experiments were conducted, 988 were successfully captured, the probability of target capture in each experiment was p = 0.9888, and the probability of success was 98.88%. According to the binomial distribution, 988 obeyed the binomial distribution with parameters of 1000 and 0.9888, the sample average was $\bar{\mu} = np = 988.8$. Calculate the confidence interval with normal distribution: assuming the confidence level is 95%, the $z_{\alpha/2} = 1.96$, the standard deviation of the sample is $\sigma = \sqrt{np(1-p)} = 3.32$. The formula for the confidence interval is:

$$p - z_{\alpha/2} \cdot \sqrt{\frac{p(1-p)}{n}} \leq p \leq p + z_{\alpha/2} \cdot \sqrt{\frac{p(1-p)}{n}} \tag{7}$$

The confidence interval obtained through calculation is [0.9822, 0.9953].

5. Discussion

Based on the TOF laser measurement system and high-speed galvanometer scanning technology, this paper focused on the target acquisition problem for an a priori moving target model with a Gaussian distribution in the threshold scanning range. To improve the scanning times of the central area, an innovative and improved hexagonal honeycomb structure scanning model was proposed. Through simulation verification, within the visual threshold range of the same frame size, the acquisition probability of the target was 3% higher than that for the traditional hexagonal spiral scanning method, 5% higher than that for rectangular spiral scanning, and 14% higher than that for rectangular branch scanning. This scanning method provides a new solution for target acquisition in laser communication, laser docking, airborne radar, and other fields.

Author Contributions: Conceptualization, B.J. and Q.L.; methodology, F.J.; software, F.J.; validation, B.J., F.J. and Y.L.; formal analysis, Q.L.; data curation, Y.L.; writing—original draft preparation, F.J.; writing—review and editing, B.J. and Q.L.; visualization, F.J.; supervision, Y.L.; project administration, B.J.; funding acquisition, Q.L. All authors have read and agreed to the published version of the manuscript.

Institutional Review Board Statement: Not applicable.

Informed Consent Statement: Not applicable.

Data Availability Statement: Not applicable.

Conflicts of Interest: The authors declare no conflict of interest.

References

1. Marshall, G.F.; Stutz, G.E. *Handbook of Optical and Laser Scanning*, 2nd ed.; Marcel Dekker Inc.: New York, NY, USA, 2012.
2. Xie, S.; Du, Y.; Zhang, Y.; Wang, Z.M.; Zhang, D.L.; He, L.; Qiu, L.P.; Jiang, J.H.; Tan, W.H. Aptamer-based optical manipulation of protein subcellular localization in cells. *Nat. Commun.* **2020**, *11*, 1347. [CrossRef] [PubMed]
3. Abouakil, F.; Meng, H.; Burcklen, M.A.; Rigneault, H.; Galland, H.; LeGoff, L. An adaptive microscope for the imaging of biological surfaces. *Light Sci. Appl.* **2021**, *10*, 210. [CrossRef] [PubMed]
4. Porfirev, A.P.; Fomchenkov, S.A. Effect of laser radiation power on laser trapping of light-absorbing microparticles in air. *Procedia Eng.* **2017**, *201*, 48–52. [CrossRef]
5. Porfirev, A.P. Experimental investigation into the possibilities of using a spatial light modulator for laser-trapping light-absorbing micro-objects in air. In Proceedings of the XIII International Scientific and Technical Conference on Optical Technologies in Telecommunications, Ufa, Russian, 11–18 November 2015. [CrossRef]
6. Küppers, M.; Albrecht, D.; Kashkanova, A.D.; Lühr, J.; Sandoghdar, V. Confocal interferometric scattering microscopy reveals 3D nanoscopic structure and dynamics in live cells. *Nat. Commun.* **2023**, *14*, 1962. [CrossRef]
7. Lu, J.S.; Wang, H.Y.; Kudo, T.; Kudo, T.; Masuhara, H. Large Submillimeter Assembly of Microparticles with Necklace-like Patterns Formed by Laser Trapping at Solution Surface. *J. Phys. Chem. Lett.* **2020**, *11*, 6057–6062. [CrossRef]
8. Espina, V.; Heiby, M.; Pierobon, M.; Liotta, L.A. Laser capture microdissection technology. *Expert Rev. Mol. Diagn.* **2007**, *7*, 647–657. [CrossRef]
9. Simone, N.L.; Bonner, R.F.; Gillespie, J.W.; Emmert-Buck, M.R.; Liotta, L.A. Laser-capture microdissection: Opening the microscopic frontier to molecular analysis. *Trends Genet.* **1998**, *14*, 272–276. [CrossRef]
10. Suarez-Quian, C.A.; Goldstein, S.R.; Pohida, T.; Smith, P.D.; Peterson, J.I.; Wellner, E.; Ghany, M.; Bonner, R.F. Laser capture microdissection of single cells from complex tissues. *Biotechniques* **1999**, *26*, 328–335. [CrossRef]
11. Klee, E.W.; Erdogan, S.; Tillmans, L.; Kosari, F.; Sun, Z.F.; Wigle, D.A.; Yang, P.; Aubry, M.C.; Vasmatzis, G. Impact of sample acquisition and linear amplification on gene expression profiling of lung adenocarcinoma: Laser capture micro-dissection cell-sampling versus bulk tissue-sampling. *BMC Med. Genom.* **2009**, *2*, 13. [CrossRef]
12. Todd, R.; Kuo, M.W.L.W.P. Gene expression profiling using laser capture microdissection. *Expert Rev. Mol. Diagn.* **2002**, *2*, 497–507. [CrossRef]
13. Priezzhev, A.; Lee, K. Potentialities of laser trapping and manipulation of blood cells in hemorheologic research. *Clin. Hemorheol. Micro.* **2016**, *64*, 587–592. [CrossRef] [PubMed]
14. Ouyang, W.; Xu, X.; Lu, W.; Zhao, N.; Han, F.; Chen, S.C. Ultrafast 3D nanofabrication via digital holography. *Nat. Commun.* **2023**, *14*, 1716. [CrossRef]
15. Yang, D.; Liu, Y.; Chen, Q.; Chen, M.; Zhan, S.D.; Cheung, N.K.; Chan, H.Y.; Wang, Z.D.; Li, W.J. Development of the high angular resolution 360° LiDAR based on scanning MEMS mirror. *Sci. Rep.* **2023**, *13*, 1540. [CrossRef] [PubMed]
16. Ravikumar, V.K.; Chin, J.M.; Lua, W.; Linarto, N.; Ranganathan, G.; Trisno, J.; Pey, K.L.; Yang, J.K.W. Super-resolution laser probing of integrated circuits using algorithmic methods. *Nat. Commun.* **2022**, *13*, 5155. [CrossRef] [PubMed]
17. Abdelmoula, M.; Zarazaga, A.M.; Küçüktürk, G.; Maury, F.; Grossin, D.; Ferrato, M. Scanning Strategy Investigation for Direct Powder Bed Selective Laser Processing of Silicon Carbide Ceramic. *Appl. Sci.* **2022**, *12*, 788. [CrossRef]
18. Almukhtar, A.; Saeed, Z.O.; Abanda, H.; Tah, J.H.M. Reality Capture of Buildings Using 3D Laser Scanners. *CivilEng* **2021**, *2*, 214–235. [CrossRef]
19. Zhao, L.; Mbachu, J.; Wang, B.; Liu, Z.; Zhang, H. Installation Quality Inspection for High Formwork Using Terrestrial Laser Scanning Technology. *Symmetry* **2022**, *14*, 377. [CrossRef]
20. Liu, H.Z.; Ji, Y.F. Effect of aberration on performance of the bit error rate in an inter-satellite coherent optical communication receiving system. *Acta Opt. Sin.* **2012**, *32*, 38–43. [CrossRef]
21. Rana, M.S.; Pota, H.R.; Petersen, I.R. Spiral scanning with improved control for faster imaging of AFM. *IEEE Trans. Nanotechnol.* **2014**, *13*, 541–550. [CrossRef]
22. Kelley, K.P.; Ziatdinov, M.; Collins, L.; Susner, M.A.; Vasudevan, R.K.; Balke, N.; Kalinin, S.V.; Jesse, S. Fast scanning probe microscopy via machine learning: Non-rectangular scans with compressed sensing and gaussian process optimization. *Small* **2020**, *16*, 2002878. [CrossRef]
23. Rana, M.S.; Pota, H.R.; Petersen, I.R. Performance of sinusoidal scanning with MPC in AFM imaging. *IEEE/ASME Trans. Mechatron.* **2014**, *20*, 73–83. [CrossRef]
24. Pota, H.; Petersen, I.R. Reduction of phase error between sinusoidal motions and vibration of a tube scanner during spiral scanning using an AFM. *Int. J. Control Autom.* **2016**, *14*, 505–513. [CrossRef]

25. Habibullah, H.; Pota, H.R.; Petersen, I.R. A novel control approach for high-precision positioning of a piezoelectric tube scanner. *IEEE Trans. Autom. Sci. Eng.* **2016**, *14*, 325–336. [CrossRef]
26. Wang, T.; Yang, S.M.; Li, S.S.; Yuan, Y.; Hu, P.Y.; Liu, T.; Jia, S.H. Error analysis and compensation of galvanometer laser scanning measurement system. *Acta Opt. Sin.* **2020**, *40*, 2315001. (In Chinese)
27. Qi, S.; Zhang, Q.; Xin, X.J.; Tao, Y.; Tian, Q.H.; Tian, F.; Cao, G.X.; Shen, Y.F.; Chen, D.; Gao, Z.H.; et al. Research on Scanning Method in Satellite Laser Communication. In Proceedings of the International Conference on Optical Communications and Networks (ICOCN), Huangshan, China, 5–8 August 2019. [CrossRef]
28. Yuan, G.F.; Ma, X.Y.; Liu, S.; Yang, Q.L. Research on Lidar scanning mode. *High Power Laser Part. Beams* **2020**, *32*, 041001-1–041001-6. (In Chinese) [CrossRef]
29. D'Agostino, F.; Ferrara, F.; Gennarelli, C.; Guerriero, R.; McBride, S.; Migliozzi, M. Fast and accurate antenna pattern evaluation from near-field data acquired via planar spiral scanning. *IEEE Trans. Antennas Propag.* **2016**, *64*, 3450–3458. [CrossRef]
30. Bucci, O.M.; D'agostino, F.; Gennarelli, C.; Riccio, G.; Savarese, C. Near-field-far-field transformation with spherical spiral scanning. *IEEE Antennas Wirel. Propag. Lett.* **2003**, *2*, 263–266. [CrossRef]
31. Candra, R.; Madenda, S.; Sudiro, S.A.; Subali, M. The implementation of an efficient zigzag scan. *JTEC* **2017**, *9*, 95–98.